Size Control of Charge-Orbital Order in Half-Doped Manganite $La_{0.5}Ca_{0.5}MnO_3$

Hena Das,[1] G. Sangiovanni,[2] A. Valli,[2] K. Held,[2] and T. Saha-Dasgupta[1,*]

[1]*S. N. Bose National Centre for Basic Sciences, Kolkata 700098, India*

[2]*Institute for Solid State Physics, Vienna University of Technology, 1040 Wien, Austria*

(Received 16 June 2011; published 4 November 2011)

Motivated by recent experimental results, we study the effect of size reduction on half-doped manganite, $La_{0.5}Ca_{0.5}MnO_3$, using the combination of density-functional theory (DFT) and dynamical mean-field theory (DMFT). We find that upon size reduction the charge-ordered antiferromagnetic phase, observed in bulk, is destabilized, giving rise to the stability of a ferromagnetic metallic state. Our theoretical results, carried out on a defect-free nanocluster in isolation, establish the structural changes that follow upon size reduction to be responsible for this. Our study further points out the effect of size reduction to be distinctively different from application of hydrostatic pressure. Interestingly, our DFT + DMFT study additionally reports the correlation-driven stability of the charge-orbitally ordered state in bulk $La_{0.5}Ca_{0.5}MnO_3$, even in the absence of long-range magnetic order.

DOI: 10.1103/PhysRevLett.107.197202 PACS numbers: 75.47.Lx, 68.65.−k, 71.15.Mb, 71.27.+a

Size controls the physical properties of materials and can hence be employed to make materials functional. For strongly correlated materials, theoretical modeling of such phenomena is rare. Here, we pursue such a study taking the case of half-doped manganites. The charge and orbitally ordered state observed in half-doped manganites is among the rich variety of fascinating phenomena exhibited by perovskite manganites $R_{1-x}A_xMnO_3$ (R represents a rare-earth-metal element and A an alkali-earth-metal element) [1]. The charge-ordered (CO) state is associated with a real space ordering of Mn^{3+}/Mn^{4+} species in a 1:1 pattern. It is accompanied by orbital ordering (OO) and a structural change from orthorhombic to monoclinic symmetry which gives rise to an insulating ground state [2–6]. The insulating CO state has been reported to be destabilized to a ferromagnetic (FM) metallic phase by various means that include a magnetic field [7], doping, biaxial strain, pressure [8], and electric field [9]. Very recently, it has been shown in a few experimental studies [10–12] that the destabilization of the CO state can be achieved even through size reduction. This interesting phenomenon adds another dimension, namely, size, to the problem. Size control is attractive from a technology point of view, which is achievable chemically in a low-cost way. The route through size control also opens up the possibility of exploring the tunability of the CO-OO state and the associated metal-insulator transition.

In this Letter, we study the effect of size reduction on the CO-OO state of $La_{0.5}Ca_{0.5}MnO_3$ (LCMO) by using a combination of first-principles density-function theory (DFT) and dynamical mean-field theory (DMFT). For the DFT calculations, we used a combination of two methods: (a) plane-wave-based pseudopotentials [13] and (b) muffin-tin orbital (MTO) based on linear muffin-tin orbital [14] and Nth order MTO (NMTO) [15]. For (a) we used projected augmented wave pseudopotentials with an energy cutoff of 450 eV. We used a spin polarized generalized gradient approximation (GGA) [16]. From a self-consistent DFT calculation, a low-energy Mn e_g only model Hamiltonian was constructed using the NMTO-downfolding technique [15]. The corresponding Hubbard Hamiltonian defined in the downfolded NMTO basis was solved using DMFT, in the same spirit as previously carried out in Ref. [17] in the context of pure $LaMnO_3$. The low-energy model Hamiltonian consists of two e_g orbitals per Mn ion with intraorbital Coulomb interaction $U = 5$ eV and Hund's exchange $J = 0.75$ eV which are coupled by $\mathcal{J} = 1.35$ eV to a (classical) spin representing the half filled and immobile t_{2g} electrons. The DMFT equations were solved by Hirsch-Fye quantum Monte Carlo simulations [18], and, because of the CO ordering, it was necessary to explicitly consider a site-dependent double counting correction [19].

Bulk LCMO shows a CO transition at $T_{CO} = 155$ K. Below 155 K, the crystal structure is of monoclinic symmetry ($P2_1/m$) and an antiferromagnetic (AFM) order sets in [20]. The magnetic structure, the so-called "CE" order, consists of zigzag FM chains that are coupled antiferromagnetically in the crystallographic ac plane. The ac planes are stacked antiferromagnetically along the crystallographic b direction. A noteworthy feature of the crystal structure is that, while the Jahn-Teller distortion is sizable for the bridge-site Mn atoms (Mn1) with two long bonds along the FM chain and four short bonds, the corner-site Mn atoms (Mn2) on the zigzag chains have negligible distortion with nearly similar Mn-O bond lengths. The average Mn2-O distance is smaller than that of Mn1-O [2]. Our DFT calculations carried out on the experimentally measured structure [2], henceforth, referred to as S_{expt}, showed the CE insulating phase to be stable by 18 meV/f.u. over the FM metallic solution. The calculated electronic structure in terms of density of states and

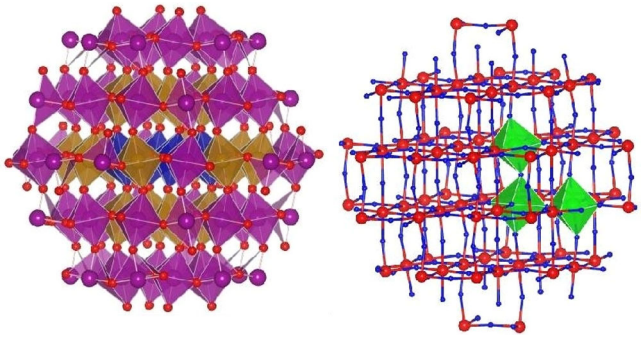

FIG. 1 (color online). Left: Constructed nanocluster of LCMO. In dark gray (magenta), light gray (brown), and dark gray (blue) we show the MnO_6 octahedra belonging to the outer most surface layer, next to the surface, and the core region. Right: The structural unit, highlighted in gray (green), chosen out of S_{nano}, used for building up of S_{model}. The big and small spheres in the unshaded region represent Mn and O atoms, respectively.

magnetic moments are found to be in good agreement with those reported previously in literature [21].

In order to study the problem of nanoscale LCMO, we first created a large supercell in the monoclinic structure, from which a cluster of diameter 2–3 nm having approximate spherical shape was cut out (cf. Fig. 1, left panel), in which we carried out a full structural optimization. Following this procedure, the 2 nm cluster contains a total of 370 atoms and the 3 nm cluster contains a total of 700 atoms, pushing it to a limit of our DFT structural optimization. In the construction of the clusters, care has been taken to maintain the stoichiometry as closely as possible. For the cluster calculation, a simple cubic supercell was used with periodic boundary conditions, where two neighboring clusters were kept separated by 10 Å, which essentially makes the interaction between cluster images negligible. The positions of the atoms were relaxed towards equilibrium, using the conjugate gradient technique until the Hellmann-Feynman forces became less than 0.001 eV/Å.

The considered DFT cluster sizes are smaller than the experimental realizations [10] of sizes 15 nm. Hence only the inner region of the above constructed clusters of 2–3 nm size is expected to mimic the prototypical behavior of the experimentally studied clusters. In order to understand the consequences of the size-controlled structural changes for such relatively larger clusters, we hence constructed a model bulk system, which we refer to as S_{model}. It is built out of the structural units belonging to the innermost core and the next to the core layer of the optimized LCMO in the nanoscale geometry (referred to as S_{nano}), as shown in the right panel of Fig. 1, and subsequently imposing the symmetry considerations. The detailed procedure of construction of the model system is explained in the Supplemental Material (SM) [22]. Construction of S_{model} leads to consideration of the local oxygen environments around Mn atoms as well as the tilt and rotation connecting two MnO_6 octahedra, the same as that in the core region of S_{nano}. The lattice parameters and the Mn-O bond lengths of S_{model} are compared to the bulk structure in Table I. The detailed structural information can be obtained in the SM [22]. Note that, for the bulk, we have considered the theoretically optimized structure, referred to as S_{bulk}, in order to compare with parameters of S_{model} on the same footing. We find that the lattice parameters of S_{model} show substantial reduction compared to those of the bulk system. The change in the a parameter appears to be the largest with a change of about 0.20 Å, with moderate changes in the b and c parameters, of 0.09 Å. Qualitatively, this trend of reduction in lattice parameters and also the nature of reduction agree very well with the crystal structure data extracted from x-ray diffraction of nanoclusters of LCMO of 15 nm size [cf. Fig 4 in Ref. [10(a)]]. We note that the reduction in lattice parameters in the model structure gave rise to about 6% reduction in the volume compared to that of the bulk system; the first experiments [10] report a 2% reduction. The 6% reduction was obtained for S_{model} constructed out of S_{nano} of 3 nm, while a similar procedure for S_{nano} of 2 nm gave rise to larger volume reduction ($\approx 8\%$). This indicates that the volume reduction increases upon decreasing cluster size, justifying the difference between the obtained volume reduction on the 2–3 nm cluster and the experimentally observed volume reduction on the 15 nm cluster. One of the important structural quantities is the orthorhombic strain: $OS_{\parallel} = 2\frac{(c-a)}{(c+a)}$ gives the strain in the ac plane, while $OS_{\perp} = 2\frac{(a+c-\sqrt{2}b)}{(a+c+\sqrt{2}b)}$ is that along the b axis. For S_{bulk}, the orthorhombic strain is highly anisotropic with a negligible value of $OS_{\parallel}$ (≈ 0.002) and a high value of $OS_{\perp}$ (≈ 0.021). For S_{model}, we find instead the orthorhombic strains to be comparable ($OS_{\parallel} \approx 0.02$ and $OS_{\perp} \approx 0.01$). This trend is also in very good agreement

TABLE I. Lattice parameters and Mn-O bond lengths (in Å) of S_{model} in comparison to S_{bulk}. The entries for the Mn-O bond length from left to right correspond to that along the FM chain, between the FM chains, along the b direction, and the average. Mn1 atoms are of nominal valence 3+ and Mn2 of 4+ [23].

	S_{bulk}				S_{model}			
Lattice parameter	$a = 5.47$, $b = 7.58$, $c = 5.48$				$a = 5.28$, $b = 7.49$, $c = 5.39$			
Mn1-O	2.18	1.93	1.94	2.02	1.97	1.92	1.91	1.93
Mn2-O	1.92	1.92	1.94	1.93	1.92	1.88	1.92	1.91

with experimental results [10]. It confirms that our constructed model structure captures the essential structural changes in the nanoscale surprisingly well. This proves that the role of surface beyond what is already taken into account in construction of the model structure is small.

Next we calculated the electronic structure for S_{model} and compared it with that of S_{bulk}. For understanding the results, let us note that the difference between the average Mn1-O and Mn2-O bond lengths is smaller in S_{model} than in S_{bulk}. This leads to the expectation that the charge disproportionation (CD) between Mn1 and Mn2 sites will decrease in S_{model}. Furthermore, we note that for S_{bulk} the difference between the longest and the shortest Mn-O bond lengths is large for Mn1 and tiny for Mn2. This gives rise to the crystal field splitting (Δ) between the two Mn e_g states, Mn $3z^2 - r^2$ and Mn $x^2 - y^2$, as large as 0.63 eV for Mn1 sites and less than 0.02 eV for the Mn2 sites. In contrast for S_{model}, the bond length differences are much more similar for both types of Mn sites. This is reflected in similar Δ's for the nanomodel, i.e., 0.15 eV for Mn1 sites and 0.10 eV for Mn2 sites. Together these two effects weaken CO as well as OO in S_{model}. This ordering is important to stabilize the AFM structure found for the bulk. With charge and orbital ordering weakened, we instead find FM to be stable by 20 meV in S_{model}. This result is in accordance with the experimental observations [10,11]. The microscopic origin of the size-controlled transition from AFM to FM, therefore, can be traced back to the size-induced structural changes.

Figure 2 shows the density of states (DOS) of S_{bulk} with AFM ordering of Mn spins, in comparison to that of S_{model} with FM ordering. Considering the DOS for S_{bulk}, the crystal field splitting between Mn $3z^2 - r^2$ and Mn $x^2 - y^2$ is clearly seen. In the majority spin channel, Mn $3z^2 - r^2$ states at the Mn1 site are more occupied than the Mn $3z^2 - r^2$ states at the Mn2 site, giving rise to CD between Mn1 and Mn2. We also find OO at the Mn1 sites with a preferential occupation of Mn $3z^2 - r^2$ over Mn $x^2 - y^2$. The CO, although incomplete, together with

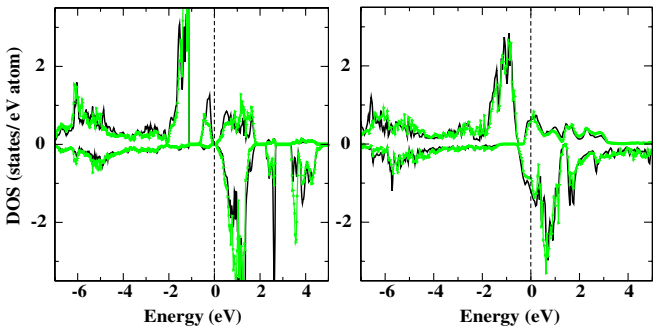

FIG. 2 (color online). DFT DOS, projected onto Mn1 d (black solid line) and Mn2 d [light gray (green) line] states calculated for the CE phase of S_{bulk} (left panel) and the FM phase of S_{model} (right panel). The zero of energy is set at E_F.

the AFM spin ordering gives rise to an insulating solution with a small but finite gap at E_F already at the DFT level. Considering the DOS of S_{model}, we find that the splitting between Mn $3z^2 - r^2$ and Mn $x^2 - y^2$ is less pronounced and the Mn1 d and Mn2 d states to be similar. The reduced Δ together with the increased bandwidth, compared to the bulk structure, drives S_{model} to metallicity with a finite density of states at the Fermi energy (E_F). The increased bandwidth is caused by the reduction in volume as well as by the FM ordering which allows hopping processes within a double exchange model [24].

In order to take into account the influence of the missing electronic correlation in GGA, we did paramagnetic DMFT calculations for S_{bulk} and S_{model} structures, considering the low-energy Mn e_g only Hamiltonian derived out of DFT. Table II lists the orbital occupations of the three types of inequivalent Mn sites. For S_{bulk}, already in the DFT (in brackets) the two inequivalent Mn1 ("Mn^{3+}-like") sites [Mn1(1) and Mn1(2)] are more occupied than the Mn2 ("Mn^{4+}-like") sites [25]. In addition to the CD, there is, as mentioned above, a DFT orbital order. Electronic correlations enhance both kinds of ordering dramatically, making CO and OO nearly complete. This establishes the correlation-driven stability of CO and OO with almost complete CD in a paramagnetic phase. The almost complete CD and enhanced orbital polarization (OP) at the Mn1 sites results in a gap at the chemical potential in the DFT + DMFT spectral function for the bulk structure, as shown in the left panel of Fig. 3, even without spin ordering. Note the opening of the charge gap is stabilized by long-range Coulomb interactions which, within DMFT, reduce to their Hartree contribution. This effect is taken into account in our DFT + DMFT calculation on the GGA level. Compared to the DFT spectra, spectral weight is transferred to high frequencies in the form of Hubbard bands, opening a gap at the chemical potential. For the DFT calculation, on the other hand, the charge disproportionation is incomplete, and the insulating solution is obtained only by assuming the AFM spin ordering. Turning to S_{model}, the DFT occupancies show Mn^{3+}-like and Mn^{4+}-like sites to be similar with only a weak CD. The inclusion of the correlation effect through DMFT enhances CD to some extent following the trend

TABLE II. Orbital occupancies for Mn $3z^2 - r^2$ (first entry) and $x^2 - y^2$ (second entry) states calculated within DFT + DMFT for different inequivalent classes of Mn atoms in the unit cell for S_{bulk} and S_{model}. In brackets we give the corresponding occupancies for the one particle, low-energy DFT Hamiltonian.

	Bulk		Nanomodel	
Mn1(1)	0.87 (0.50)	0.01 (0.11)	0.52 (0.31)	0.09 (0.20)
Mn1(2)	0.85 (0.47)	0.01 (0.12)	0.72 (0.38)	0.04 (0.19)
Mn2	0.04 (0.15)	0.09 (0.25)	0.16(0.21)	0.16 (0.25)

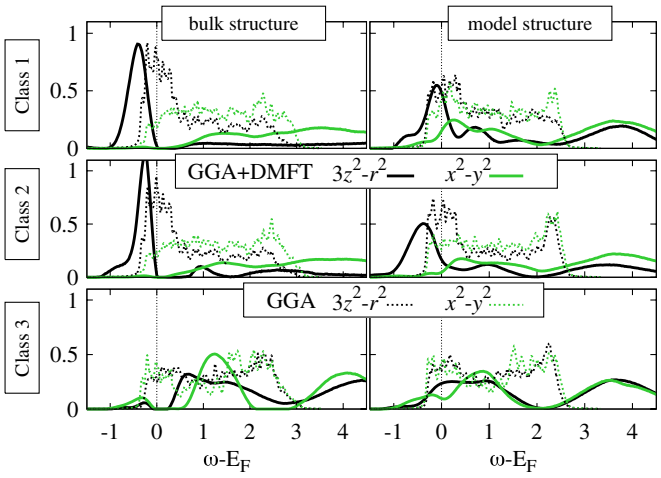

FIG. 3 (color online). DFT + DMFT spectral densities for e_g states of three inequivalent classes of Mn (solid lines), corresponding to S_{bulk} and S_{model}. The dashed lines represent the corresponding DFT DOS. The lines colored as black and light gray (green) correspond to $3z^2 - r^2$ and $x^2 - y^2$ states, respectively.

seen for S_{bulk}. However, CD remains incomplete with an average occupation of Mn^{3+}-like and Mn^{4+}-like sites of 0.6–0.7 and 0.3, respectively, in comparison to 0.9 and 0.1, respectively, obtained for S_{bulk}. This conclusively establishes that size reduction leads to weakening of charge disproportionation. This in turn leads to a metallic DFT + DMFT solution for S_{model} with finite weight at the chemical potential, as shown in the right panel of Fig. 3. Note that, although S_{nano} does not maintain strict stoichiometry, the constructed S_{model} is strictly stoichiometric, pointing to the fact that destabilization of CO is driven by the structural changes due to size confinement, rather than due to deviation from half-doping.

As one of the major structural changes upon size reduction is the volume compression, it is worthwhile to compare the structural and electronic changes induced by size reduction to those occurring under hydrostatic pressure. To this end, we carried out calculations of LCMO, with uniformly reduced lattice parameters with 6% reduced volume, the atomic positions being optimized in DFT, referred to as structure S_{press}. The details of the optimized structure are given in the SM [22]. Following the self-consistent DFT calculations on S_{press}, the Mn e_g only low-energy Hamiltonian was constructed and the corresponding Hubbard Hamiltonian was solved using DMFT. Compared to S_{model}, first of all, we find that at the DFT level CD and OP are much weaker, even though the volume is the same. With this less polarized starting point, all Mn sites are filled with ≈ 0.5 electrons. In this situation, electronic correlations are less relevant. The DMFT orbital and site occupations remain very similar to the DFT values with 0.4–0.6 electrons per site, and the system is far away from a metal-insulator transition (MIT). This leads us to conclude that the nanoscopic system is much closer to a MIT than bulk $La_{0.5}Ca_{0.5}MnO_3$ under hydrostatic pressure [26]. The size reduction and application of hydrostatic pressure, therefore, should be considered as two very different routes.

In conclusion, using DFT calculations combined with DMFT, we have studied the effect of size reduction on charge-orbital order in half-doped LCMO manganites. Our study indicates that the size reduction leads to substantial reduction in volume as well as a change in the nature of the orthorhombic strain. The structural changes under size reduction lead to a weakening of both charge and orbital ordering, making the ferromagnetic metallic state energetically favorable compared to the CE-type antiferromagnetic insulating state, which is the ground state of the bulk structure. While such effect has been observed, the experimental situation is faced with difficulties, like the possible presence of impure phases, the grain boundaries, nonstoichiometry. Our theoretical calculations were carried out considering nanocluster in isolation, and, therefore, devoid of such complications. Through construction of the model structure, the issue of nonstoichiometry was avoided. Furthermore, the effect of size reduction turned out to be very different from that of pure hydrostatic pressure. We predict the nanoscopic system to be close to the MIT in comparison to the system under hydrostatic pressure with the same amount of volume reduction. Increasing the size of the nanocluster, one would expect to drive the system closer and closer to MIT. It would therefore be possible to tune the LCMO system to the verge of MIT, and thereby achieve a large magnetoresistive response under small magnetic fields. Finally, while we carried out our investigation on LCMO, destabilization has been predicted for $Pr_{0.5}Ca_{0.5}MnO_3$ too [27], hinting that the observed effect is a more general one. This will be taken up in a later study.

We thank A. K. Raychaudhuri and T. Sarkar for bringing this problem to our attention, the EU-Indian network MONANI, SFB ViCom F41, and Austrian Science Fund (FWF) Grants No. GK W004 (A. V.) and No. M1136 (G. S.) for financial support. Calculations have been done on the Vienna Scientific Cluster.

*Corresponding author.
tanusri@bose.res.in

[1] Y. Tokura, *Colossal Magnetoresistive Oxides* (Gordon and Breach, New York, 2000).
[2] P. G. Radaelli *et al.*, Phys. Rev. B **55**, 3015 (1997).
[3] M. Tokunaga *et al.*, Phys. Rev. B **57**, 5259 (1998).
[4] M. M. Savosta *et al.*, Phys. Rev. B **65**, 224418 (2002).
[5] J. P. Joshi *et al.*, Phys. Rev. B **65**, 024410 (2001).
[6] J. P. Joshi *et al.*, J. Magn. Magn. Mater. **279**, 91 (2004).
[7] H. Kuwahara *et al.*, Science **270**, 961 (1995).
[8] D. P. Kozlenko *et al.*, J. Phys. Condens. Matter **16**, 5883 (2004).
[9] A. Asamitsu *et al.*, Nature (London) **388**, 50 (1997).

[10] (a) T. Sarkar *et al.*, Phys. Rev. B **77**, 235112 (2008); (b) T. Sarkar *et al.*, Appl. Phys. Lett. **92**, 123104 (2008).
[11] S. S. Rao *et al.*, Appl. Phys. Lett. **87**, 182503 (2005).
[12] T. Sarkar *et al.*, J. Appl. Phys. **101**, 124307 (2007).
[13] G. Kresse and J. Furthmüller, Phys. Rev. B **54**, 11 169 (1996).
[14] O. K. Andersen, Phys. Rev. B **12**, 3060 (1975).
[15] O. K. Andersen and T. Saha-Dasgupta, Phys. Rev. B **62**, R16 219 (2000).
[16] J. P. Perdew, K. Burke, and M. Ernzerhof, Phys. Rev. Lett. **77**, 3865 (1996).
[17] A. Yamasaki *et al.*, Phys. Rev. Lett. **96**, 166401 (2006); Y.-F. Yang and K. Held, Phys. Rev. B **76**, 212401 (2007); **82**, 195109 (2010).
[18] J. E. Hirsch and R. M. Fye, Phys. Rev. Lett. **56**, 2521 (1986).
[19] V. I. Anisimov, J. Zaanen, and O. K. Andersen, Phys. Rev. B **44**, 943 (1991).
[20] E. O. Wollan and W. C. Köhler, Phys. Rev. **100**, 545 (1955).
[21] P. K. de Boer *et al.*, Solid State Commun. **102**, 621 (1997).
[22] See Supplemental Material at http://link.aps.org/supplemental/10.1103/PhysRevLett.107.197202 for details on the crystal structures as well as on construction of the model structure.
[23] There are three inequivalent classes of Mn atoms in the unit cell, the first two are of nominal valence 3+ and the last one is of 4 + . The structural parameters corresponding to only the first Mn^{3+} is shown. Also, for the Mn^{4+} type three bond lengths are shown, taking the average of the pairs in the mentioned directions. For details see Table 2 of the SM [22].
[24] P. W. Anderson and H. Hasegawa, Phys. Rev. **100**, 675 (1955); P.-G. de Gennes, Phys. Rev. **118**, 141 (1960).
[25] Calculation of CD in $Pr_{0.5}Ca_{0.5}MnO_3$ by V. I. Anisimov *et al.* [Phys. Rev. B **55**, 15494 (1997)] showed negligible CD. The CD obtained in the present case is presumably driven by the significant Jahn-Teller effect at the Mn1 site.
[26] Although compression of volume and Mn-O bonds happens both in nanoscale and on the application of pressure, the larger $OS_{\|}$ in the case of nanoscale compared to that under pressure makes the Mn e_g bandwidth smaller for the former, through reduction in Mn-O-Mn bond angle.
[27] T. Sarkar *et al.*, J. Appl. Phys. **101**, 124307 (2007).